ACS APPLIED MATERIALS & INTERFACES

Research Article

www.acsami.org

On-Demand Gas-to-Liquid Process To Fabricate Thermoresponsive Antimicrobial Nanocomposites and Coatings

Bijay Kumar Poudel,[†] Jae Hong Park,[*,‡] and Jeong Hoon Byeon[*,†]

[†]School of Mechanical Engineering, Yeungnam University, Gyeongsan 38541, Republic of Korea

[‡]School of Health Sciences, Purdue University, West Lafayette, Indiana 47907, United States

Supporting Information

ABSTRACT: Antimicrobial material is emerging as a major component of the mitigation strategy against microbial growth on abiotic surfaces. In this work, a newly designed process is proposed to fabricate thermoresponsive antimicrobial nanocomposites (TANs) and coatings (TACs) as an on-demand system. Thermoresponsive polymer (TRP)-incorporated silver (Ag) nanocomposites with silica nanoparticles (SNPs) or carbon nanotubes (CNTs; Ag-SNP@TRP or Ag-CNT@TRP) were produced by a single-pass gas-to-liquid process. The SNPs or CNTs were first produced by spark ablation and successively injected for dispersal in a liquid cell containing polydimethylsiloxane, poly(*N*-isopropylacrylamide), and silver nitrate under ultrasound irradiation. Suspensions of Ag-SNP@TRP or Ag-CNT@TRP nanocomposites were then deposited on a touch screen panel (TSP) protection film via electrohydrodynamic spray to form transparent antibacterial coatings. Fundamental antibacterial activities of TANs were evaluated against *Escherichia coli* and *Staphylococcus epidermidis*. The TANs showed stronger antibacterial activities at the higher temperature for all testing conditions. Lower minimum inhibitory concentrations of Ag-SNP@TRP and Ag-CNT@TRP nanocomposites were required against the two bacteria at 37 °C compared to those at 27 °C. The TACs on display showed elevated antimicrobial activity when the panel was turned on (38.1 °C) compared with when the panel was turned off (23.8 °C). This work provides a utilizable concept to continuously fabricate TANs and TACs, and it specifically offers stimuli-sensitive control of antimicrobial activity on TSPs, including other frequently touched surfaces.

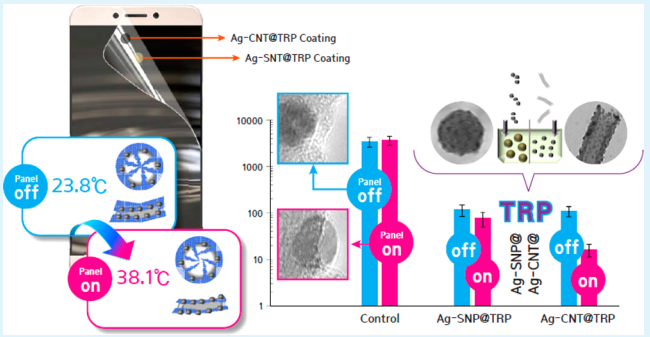

KEYWORDS: *thermoresponsive nanocomposites, thermoresponsive coatings, on-demand system, single-pass gas-to-liquid process, touch screen panel protection film, antimicrobial activities*

1. INTRODUCTION

Handheld electronic devices such as mobile phones and tablet computers have been reported to harbor clinically significant pathogens.[1] In healthcare settings, these devices may serve as a source of cross-contamination and nosocomial transmission of pathogens between individuals.[2] These devices are not subjected to routine disinfection within hospitals and homes because of the absence of disinfecting protocols for easily water-damageable and fragile electronic devices.[3] To overcome these problems, researchers have proposed antimicrobial coatings that can prevent microbial adhesion and growth via close contact between antimicrobial agent and bacteria, microbes-repelling (i.e., polymeric coatings to prevent bacterial attachment), or antimicrobial agent releasing.[4−9] Release-based antimicrobial coatings are most common, and they exert their antibacterial activity by eluting the antibiotics to the interface in a concentration-gradient dependent manner. However, these coatings have a limited reservoir of antimicrobial compounds that gradually become exhausted.[10] As the concentration of antimicrobial agent decreases to subinhibitory level, the microbes may develop resistance overtime. These issues with antibiotics might be addressed using Ag nanoparticles (NPs).

AgNPs show significant activity against a broad spectrum of Gram-positive and -negative bacteria.[11] The NPs have been engineered for specific use in a wide range of daily life, industrial, and technological applications. AgNPs can be incorporated in antimicrobial coatings and used as a durable reservoir for the sustained release of antibacterial Ag ions (Ag^+).[12] AgNPs have introduced minimal clinical incidence to bacterial resistance, which might be caused by the multiplicity of intracellular targets of Ag^+ in bacteria.[13] A previous study reported that a silicon matrix impregnated with AgNPs prevents bacterial adhesion and growth.[14] More recently, however, adverse or toxic effects on human health have significantly been considered for their efficient realistic applications compared with other antibiotics.[15] The toxicity of AgNPs can be minimized via surface modification with biocompatible materials or by embedding them in a supporting matrix or substrate.[16,17]

Received: April 12, 2017
Accepted: April 19, 2017
Published: April 19, 2017

DOI: 10.1021/acsami.7b05167
ACS Appl. Mater. Interfaces 2017, 9, 15342−15349

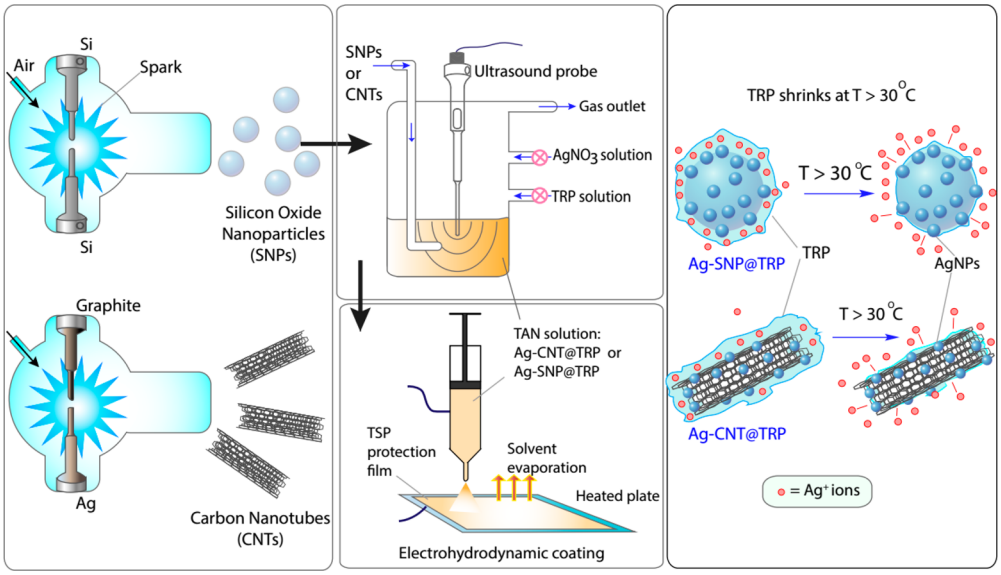

Figure 1. Schematic of single-pass gas-to-liquid process for continuous fabrication of Ag-SNP@TRP and Ag-CNT@TRP nanocomposites with spark ablation (Si or graphite-Ag electrodes), Ag(I)-TRP cell connected with probe sonicator, and in-house built electrohydrodynamic spray device connected in series.

AgNPs are commonly prepared as colloidal dispersion by hydrothermal processes based on chemical reduction of aqueous Ag^+. Surfactants are usually required to stabilize the newly formed AgNPs by providing identical electrostatic charges (to induce repulsive forces) on their surfaces that prevent unwanted aggregation or agglomeration between the NPs. However, the properties of surfactants can be changed or deteriorated when they are exposed to different physical conditions for a certain time; thus, the dispersity of NPs can be unstable over time.[18,19] The agglomerates of AgNPs cause the reduction in antimicrobial activity because AgNPs are known to exhibit size-dependent interaction with bacteria.[20] To achieve long-term stability of AgNPs without significant decreases in antibacterial activity, further utilizable fabrication approaches need to be developed. Many researchers have employed carbon or silica as supporting materials to fabricate AgNP-loaded antimicrobial nanocomposites.[21−23] Carbon nanotubes (CNTs) and silicon nanoparticles (SNPs) serve as effective supporting material because of their high surface area and chemical stability. AgNP-incorporated CNTs enhance antimicrobial activities against bacteria, such as *Pseudomonas aeruginosa*, *Staphylococcus aureus*, and *Sphingomonas spp.*, and also reduce cytotoxicity to mammalian cells when compared with AgNPs alone.[11,24] The incorporation of AgNPs with biocompatible materials reduces toxicity of AgNPs to mammalian cells because direct contact of the NPs to cells is hindered by passivating the surfaces.[17] Surface coatings of AgNPs with biocompatible polymers have also been considered to control bursting Ag^+ diffusion for reducing toxic effects on mammalian cells.[16]

Thermoresponsive polymers (TRPs), such as poly(*N*-isopropylacrylamide; PNIPAM) and poly(*N*-vinylcaprolactam), have been employed as smart polymers to modulate the release kinetics of drugs and genetic materials in response to changes in temperature.[25−27] Recently, TRPs have also been engineered to develop thermoresponsive antimicrobial coatings. Copolymers with antimicrobial agents were employed to derive thermoresponsive antimicrobial activity. The copolymers underwent conformational change to promote exposure of antimicrobial agents to bacteria below transition temperature.[28,29] PNIPAM has a lower critical solution temperature (LCST) of 32 °C, which is close to physiological temperature (37 °C). Above LCST, PNIPAM undergoes reversible phase transition from random coil conformation to compressed globular conformation, thereby effectively decreasing its volume and releasing its contents.[30] A previous report introduced AgNPs-incorporated PNIPAM as nanogels to be coated on fibrous substrates for thermoresponsive antimicrobial activity against bacteria.[31] TRPs can be used for coating AgNPs, implying that the Ag^+ release from underlying AgNPs can be triggered by externally applied heat. This feature would be efficiently applicable for electronic devices, which heat up when turned on and from heat transfer by touching. This unique feature also helps extend the duration of sustained release of Ag^+ because it minimizes the nontriggered background leaching of Ag^+ from AgNPs.

In the present work, a newly designed process is proposed to fabricate thermoresponsive antimicrobial nanocomposites (TANs) and coatings (TACs) as an on-demand system, as shown in Figure 1. TRP-incorporated Ag nanocomposites with SNPs or CNTs (i.e., Ag-SNP@TRP or Ag-CNT@TRP) were fabricated by single-pass gas-to-liquid process. The SNPs or CNTs[32] were produced by spark ablation (operating conditions are described in Table S1 of the Supporting Information) and successively injected for dispersal in a liquid cell containing polydimethylsiloxane (PDMS), PNIPAM, and silver nitrate under ultrasound irradiation. The cell contained a biphasic mixture of (a) aqueous $AgNO_3$ solution, which acted as AgNPs precursor, and (b) polymeric solution of PNIPAM and PDMS in dichloromethane, which acted as both reducing and thermoresponsive passivating agents. AgNPs were produced by the reduction of Ag^+ with hydrated electrons and TRP components in the presence of ultrasound, and they were subsequently attached onto the surface of SNPs or CNTs to form Ag-SNP@TRP and Ag-CNT@TRP nanocomposites. They were then deposited using an electrohydrodynamic spray to form transparent coatings on a touch screen panel (TSP) protection film. Antimicrobial activities of the TANs and

DOI: 10.1021/acsami.7b05167
ACS Appl. Mater. Interfaces 2017, 9, 15342−15349

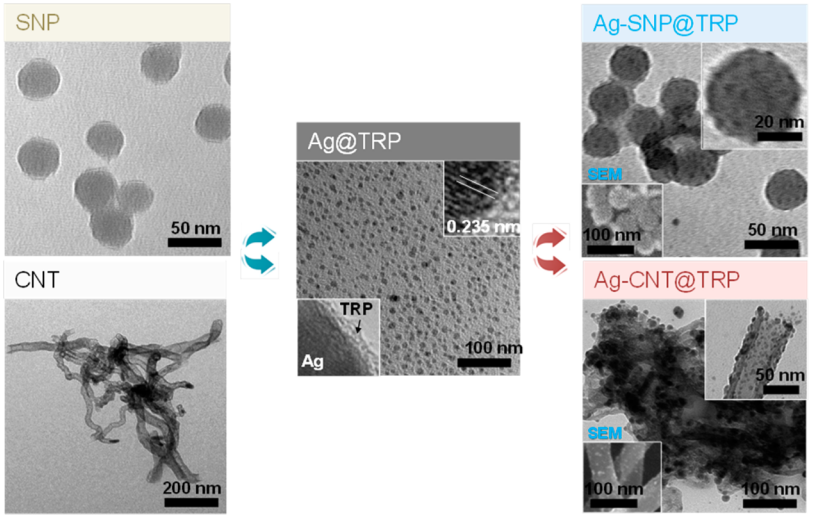

Figure 2. TEM images of spark-produced SNPs and CNTs (left), ultrasonically synthesized Ag@TRP nanoparticles (middle, inset images show TRP shell over high-magnification image of Ag, and Ag lattice), Ag-SNP@TRP nanocomposite (inset images show high-magnification image of Ag-SNP@TRP with surface-distributed darker AgNPs; SEM image of the same), and Ag-CNT@TRP nanocomposite (inset images show high-magnification image of Ag-CNT@TRP with surface-distributed darker AgNPs; SEM images of Ag-SNP@TRP and Ag-CNT@TRP).

TACs were evaluated with *Escherichia coli (E. coli)* and *Staphylococcus epidermidis* (*S. epidermidis*). Cytotoxic effects in human embryonic kidney (HEK) 293 cell were also determined using 3-(4,5-dimethylthiazol-2-yl)-5-(3-carboxymethoxyphenyl)-2-(4-sulfophenyl)-2*H*-tetrazolium (MTS) assay.

2. RESULTS AND DISCUSSION

2.1. Characterization of Fabricated Ag-SNP@TRP and Ag-CNT@TRP Nanocomposites. Morphologies of SNPs, CNTs, Ag@TRP, Ag-SNP@TRP, and Ag-CNT@TRP nanocomposites were analyzed by transmission electron microscopy (TEM). As shown in Figure 2 (left), the primary SNPs had a smooth surface and they were spherical and discrete because of unipolar charges on their surfaces (from aerosol electrometer measurements). Meanwhile, CNTs were bundled probably because of their lengthy structure with Brownian movement, although they also have unipolar surface charges. The TEM image (middle) reveals the formation of well-separated Ag@TRP in the presence of ultrasound that enhanced the isolation of AgNPs from agglomeration. As shown in the higher resolution inset images of Ag@TRP, a dark-contrast spherical particle was covered with lighter-contrast corona, which could be attributed to TRP layers. The particle showed 0.235 nm face-centered-cubic (fcc) lattice, which corresponded to the Miller plane (111) of crystalline Ag, implying that the electrons and anionic components from TRP-reduced Ag^+ to AgNPs in the presence of ultrasound. The TEM image (right) of Ag-SNP@TRP shows randomly distributed darker dots (i.e., Ag particles) on SNPs, and this finding can be verified by comparing pure SNPs, which are less electron dense compared with the darker dots in Ag@TRP and Ag-SNP@TRP samples. The gel-like TRP incorporation with Ag-dotted SNPs or individual AgNPs and SNPs as hybrid droplets during electrohydrodynamic spray-induced nanobunches by gathering of TRP, AgNPs, and SNPs due to surface tension of the hybrid droplets. In Ag-CNT@TRP sample, TRP incorporation showed an analogous tendency, which was derived from bundling of Ag-distributed CNTs. The inset scanning electron microscopy (SEM, Nova NanoSEM, FEI, USA) images of Ag-SNP@TRP and Ag-CNT@TRP samples further clarified the feasibility of the single-pass gas (SNP or CNT)-to-liquid (Ag^+ in TRP matrix) process to fabricate desired hierarchical nanostructures without any interruptions and batch steps. In addition, the mass fractions of Ag-SNP and Ag-CNT in the nanocomposites were measured using a piezobalance particle monitor (3522, Kanomax, Japan) to be 0.51 and 0.46, respectively.

The incorporation between SNPs or CNTs and Ag@TRP was further examined via X-ray diffraction (XRD), X-ray photoelectron spectra (XPS), UV−vis absorption spectra, and Fourier transform infrared (FTIR) spectra measurements. As shown in Figure S1a, the diffraction pattern of Ag-SNP@TRP revealed a broad peak at $2\theta = 22°$, representing amorphous silica along with four other peaks that were assigned to the (111), (200), (220), and (311) reflections of the fcc structure (JCPDS No. 04-0783) of crystalline AgNPs. Analogous reflections corresponding to the planes of fcc Ag structure were observed in the Ag-CNT@TRP sample, and these reflections were along the broad peak around at $2\theta = 27°$ corresponding to the graphitic structure in CNTs. The core level Ag 3d signals from XPS measurements of the Ag-SNP@TRP sample showed two characteristic peaks centered at 367.8 and 373.8 eV corresponding to Ag $3d_{5/2}$ and Ag $3d_{3/2}$, respectively, showing a slightly downward shift in binding energy compared with reference values of Ag (Figure S1b). This finding might be due to junctions from sonochemical deposition of elemental Ag on SNPs, resulting in the electron transfer from SNPs to AgNPs because they have different Fermi energy levels. This result was consistent with the spin energy separation of 6 eV, which signified the presence of zerovalent Ag in the sample.[33] The inset of Figure S1b (top) shows the wide spectrum of Ag-SNP@TRP that have characteristic peaks attributable to Ag (from AgNPs), Si and O (from SNPs), and C (from TRP layers). The spectrum for the Ag-CNT@TRP sample (Figure S1b) contained a peak with higher intensity for C elements, which was caused by CNTs that mainly consisted of graphitic carbon. In Figure S2a, the Ag-SNP@TRP or Ag-CNT@TRP nanocomposites exhibited absorbance maxima at around 420 nm in the UV−vis spectra; this finding represented the localized surface plasmon resonance characteristics of

DOI: 10.1021/acsami.7b05167
ACS Appl. Mater. Interfaces 2017, 9, 15342−15349

plasmonic AgNPs, and these features were absent in the spectra for SNPs or CNTs alone (Figure S2a). Upon an increase in temperature of nanocomposite suspension from 27 to 37 °C, the peaks of both nanocomposites broadened and simultaneously red-shifted to around 450 nm, which may be caused by shrinkage of TRP that induced an alternation of refractive index of the nanocomposites in the suspensions.[34] In the inset of Figure S2b (FTIR spectra), the absorption band of SNP at around 785 cm^{-1} could be assigned to the symmetric vibration of Si−O, whereas that at around 945 cm^{-1} was assigned to the asymmetric vibration of Si−O. The other bands between 800 and 1000 cm^{-1} could be explained as superimpositions between various SiO_2 peaks and Si−OH bonds. Meanwhile, CNTs mostly showed featureless spectrum in the tested IR range and demonstrated only a broad minor peak at around 1770 cm^{-1}, which was attributable to a C═O vibration; these results were consistent with the spectra in a previous report.[35] In Figure S2b, the bands for Ag-CNT@TRP and Ag-SP@TRP samples showed some vibration bands of Si−O, which were due to the presence of PDMS in TRP. The spectra of both nanocomposites showed $-CH_2$ groups (1460 cm^{-1}) and NH−CO groups (1550 cm^{-1}) of PNIPAM, thereby implying that both supporting SNPs and CNTs were well incorporated with TRP during the ultrasonic reactions. Distinguishable characteristic peaks for PNIPAM and PDMS implies no significant coverages by AgNPs on the outermost layer of the nanocomposites instead of TRP because AgNPs may weaken the intensity of the peaks of TRP in the measurement.

To verify the hydrosolization of gas-phase-produced SNPs and CNTs in the liquid cell (containing Ag^+, PNIPAM, and PDMS) as the supporting materials of Ag@TRP, the scanning mobility particle sizer (SMPS) was employed to measure the geometric mean diameter (GMD), geometric standard deviation (GSD), and total number concentration (TNC) of the SNPs and CNTs with and without ultrasonic irradiation. The size distributions and detailed information are displayed in Figure S3a and Table S2. Specifically, the TNC of the SNPs and CNTs after the cell in the absence of ultrasound were not significantly decreased compared with the original TNC before the injection into the cell. Thus, nearly all SNPs or CNTs flowed out from the cell along with bubbles from carrier gases. In the presence of ultrasound, the bubbles containing SNPs or CNTs imploded and/or became significantly smaller before they exited the cell, which induced collisions between SNPs or CNTs and liquid interfaces, resulting in hydrosolization with high collection efficiencies (95.54% for SNPs and 98.32% for CNTs). To examine the thermoresponsive behavior of the fabricated nanocomposites, the SMPS was further employed to measure the GMD, GSD, and TNC of the nanocomposites at two gas temperatures, namely, 27 and 37 °C. As shown in Figure 3, the GMD and TNC of Ag-SNP@TRP at 27 °C were 51 ± 2 nm and 1.45 × 10^6 particles cm^{-3}, respectively, and those were 40 ± 2 nm and 1.10 × 10^6 particles cm^{-3} at 37 °C, respectively. The identical increase in gas temperature introduced a similar tendency (the GMD and TNC are noted in Table S2) with the Ag-CNT@TRP nanoscomposites. These thermoresponsive behaviors are summarized in the inset of Figure 3, in which the equivalent mobility diameters measured using SMPS are plotted as a function of the gas temperature. Decreases in GMD and TNC by increasing the gas temperature may be due to two subsequent steps, namely, Brownian agglomeration (decreasing TNC) and successive shrinkage (decreasing GMD). Even though the increase in gas

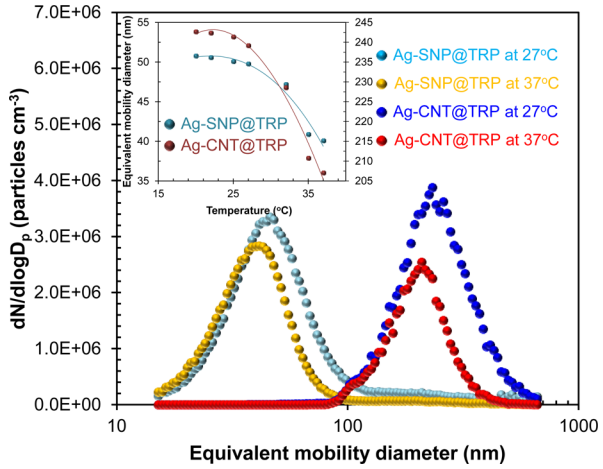

Figure 3. Particle size distributions of aerosolized Ag-SNP@TRP and Ag-CNT@TRP nanocomposites at 27 and 37 °C in gas temperature.

temperature generally induces a frequency of thermal collision between particles in the gas phase, the decreases in GMD of nanocomposites are still maintained because of shrinkages of PNIPAM that constitutes TRP enveloping nanocomposites. At temperature increases above its LCST (~32 °C), the PNIPAM collapses from random coil to globule state probably because of the destruction of hydrogen bonds between carbonyl oxygen groups of PNIPAM and adsorbed water molecules, leading to both a shrinkage in morphology and a decrease in size. Thermoresponsive behavior for TRP alone was also measured using SMPS, and the size distributions and detailed information are displayed in Figure S3b and Table S2. The results were consistent with the nanocomposites at an identical increase in gas temperature. This finding indicated that the heterogeneous conjugation between PNIPAM and PDMS in the presence of ultrasound could induce the desired thermoresponsive behavior, and this tendency could be extended to their further incorporation with other components (Ag-SNP and Ag-CNT).

2.2. Antimicrobial Activity and Cytotoxicity. The antibacterial activity of Ag-SNP@TRP and Ag-CNT@TRP nanocomposites was evaluated with *S. epidermidis* and *E. coli*. The nanocomposites were applied to Luria broth containing 10^6 colony forming unit (CFU) mL^{-1} of bacteria for 6−1440 min. The antibacterial activities for the different temperatures (27 and 37 °C) were estimated by comparing the bacterial growth between the absence and presence of TANs at a chosen temperature to compensate the different bacterial cell activities at different temperatures (refer to the Supporting Information). As shown in Figure 4a,b, cell viability significantly decreased with increasing exposure time of the nanocomposites because the water in the media may facilitate the release of Ag^+ and their subsequent diffusion to the bacteria by increasing the time. The temperature increase from 27 to 37 °C also affected the change in cell viability, which may be due to an enhancement in the degree of AgNP surface exposure to media by shrinking the TRP layer on AgNP (refer to the right-top image in Figure 1). This result implies that TRP incorporation on AgNPs could introduce an antimicrobial platform with controllable activity. The magnitude of change in antimicrobial activity for the Ag-CNT@TRP sample was bigger than that for Ag-SNP@TRP, which may be caused by different capillary suction forces of the supporting materials (i.e., SNPs and CNTs). Adsorption isotherm measurements (Figure S4)

DOI: 10.1021/acsami.7b05167
ACS Appl. Mater. Interfaces 2017, 9, 15342−15349

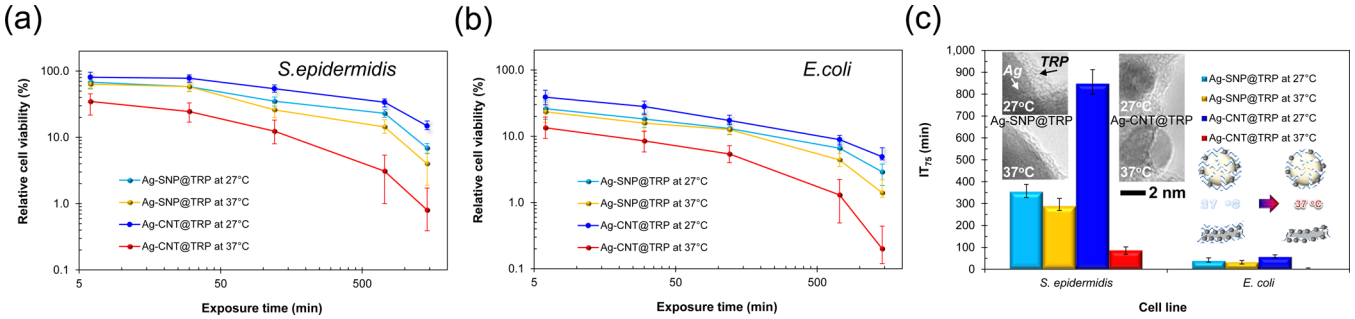

Figure 4. Cell viability versus exposure time curves of (a) *S. epidermidis* and (b) *E. coli* when exposed to Ag-SNP@TRP and Ag-CNT@TRP nanocomposites at 27 and 37 °C. (c) IT_{75} (the required time to inhibit 75% of cell proliferation) graph (inset scheme and TEM images show shrinkage of TRP shell over AgNPs when temperature increased from 27 to 37 °C).

revealed that the CNTs showed a sharp increase in $P\ P_0^{-1}$ ranging from 0.9 to 1.0, which was more suitable to have strong capillary condensation at the temperature increase (from 27 to 37 °C) because the interfacial energy between porous media and fluids decreases with decreasing pore diameter.[36] The natural antimicrobial property of CNTs might also affect the differences caused by the temperature increase and enhance the direct exposure of CNT surface to the bacteria.[37] *E. coli* was more sensitive to the antibacterial activity of the nanocomposites compared with *S. epidermidis*. Gram-positive *Staphylococcus* species have thicker and more complex peptidoglycan layers than Gram-negative *E. coli*, resulting in a stronger inhibition to Ag^+ permeability to the underlying cell membrane and cytoplasm.[38] The results are quantitatively summarized as the required time to inhibit 75% of cell proliferation (IT_{75}, Figure 4c), and the exposure of AgNPs on SNPs and CNTs via TRP shrinkage is both schematically and experimentally (TEM measurements) displayed in the inset of Figure 4c. Even though complete coverage of AgNPs by TRP (causing resistance for Ag^+ release) existed after TRP shrinkage, the Ag^+ release from exposed surfaces [the ratios between exposed length of AgNPs and perimeter of an TAN at 37 °C: 0.16 for Ag-SNP@TRP (from 0.06 at 27 °C) and 0.37 for Ag-CNT@TRP (from 0.11 at 27 °C), counted 400 particles for each in TEM analyses] could induce the better inhibition of bacterial growth (refer to Figure S5). Easy diffusion of Ag^+ to the bacterial cells was observed, which introduced strong inhibitions at the experiments. The minimum inhibitory concentrations (MICs) are described in Table S3, and the data were consistent with the results regarding supporting materials (SNP vs CNT), bacteria (*S. epidermidis* vs *E. coli*), and temperature (27 vs 37 °C).

To verify the feasibility of the nanocomposites, electrohydrodynamic spray was employed to fabricate transparent TACs (~5 μm thickness) on TSP protection films. The Ag^+ release in water from the nanocomposite-coated films was first evaluated at 27 and 37 °C (Figure 5a). The two temperatures were chosen by considering two different situations of a TSP, where one is turned off (27 °C, the lower frequency of the touching panel) and the other is continuously turned on for 15 min (37 °C, the higher frequency of the touching panel). The release amounts at 37 °C for both samples were higher than those at 27 °C, and these results would support Ag^+ diffusion to the bacteria in the presence of water molecules. The TACs on the protection films (Figure 5b) were employed to measure relative opacity (the measure of relative light transmission) using a CL-200A Minolta handheld chromameter. The values were 13.66 and 20.94 for Ag-SNP@TRP and Ag-CNT@SRP,

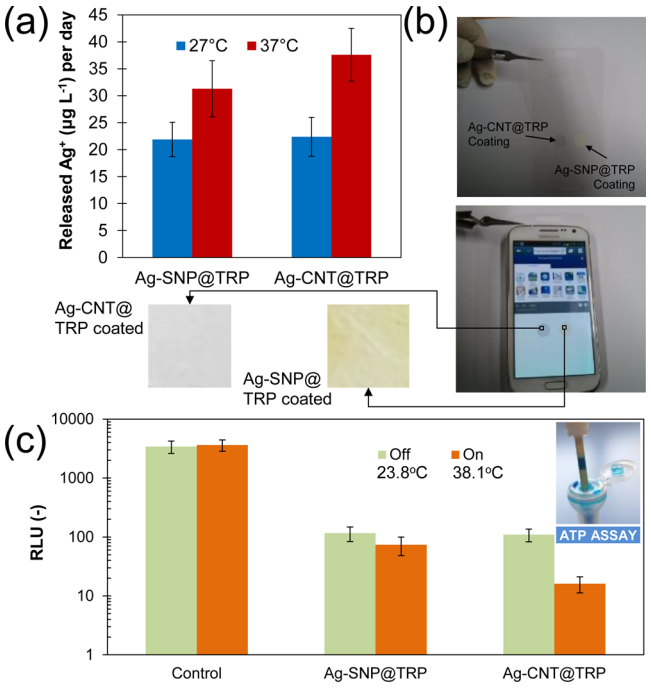

Figure 5. (a) Amounts of Ag^+ released per day from Ag-SNP@TRP and Ag-CNT@TRP nanocomposites at 27 and 37 °C. (b) Photographs of TSP protection film electrosprayed with transparent coatings of Ag-SNP@TRP and Ag-CNT@TRP nanocomposites. (c) Results of ATP assay with *E. coli* for TAC applied films on TSP with on and off modes.

respectively, and their haze (the measure of forward light scattering) values were 3.96% and 4.44%, respectively. The optical transmittance (Figure S6) of TACs (~5 μm thickness) on TSP panel protection films was also measured using a UV−vis spectrometer (UV-1800, Shimadzu, Japan) with a film holder. The transmittances of Ag-SNP@TRP- and Ag-CNT@TRP-coated films at wavelengths of 400−900 nm were 82.4% and 84.8%, respectively. Even though the films tended to become pale yellow or gray as the thickness of coating increases, the transmittances could be controlled above 80% in the visible region. Figure 5b also shows that the TACs on TSP were transparent, and the TACs displayed different transparency, opacity, and haze values. An adenosine triphosphate (ATP) test kit was employed to confirm thermoresponsive antimicrobial activity of TACs on the protection films that presented relative luminescence unit (RLU), which was relevant to CFU. *E. coli* spread on a noncoated film, used as

DOI: 10.1021/acsami.7b05167
ACS Appl. Mater. Interfaces 2017, 9, 15342−15349

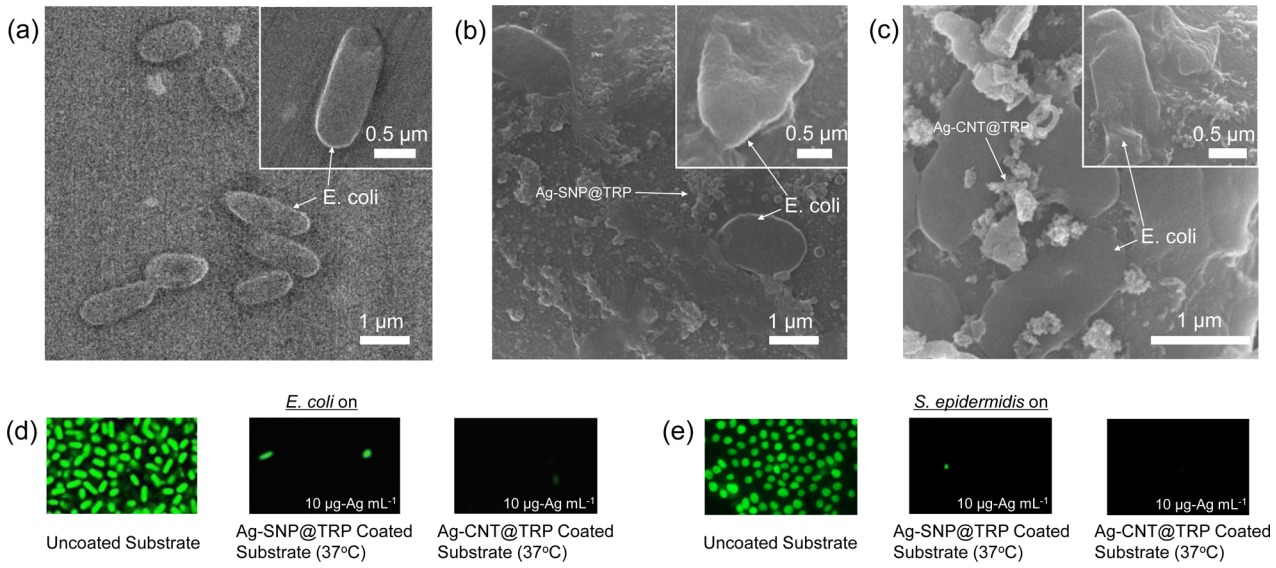

Figure 6. Low- and high-magnification SEM images of *E. coli* for untreated (a) and treated with Ag-SNP@TRP (b) and Ag-CNT@TRP (c). CLSM images of living (green) *E. coli* (d) and *S. epidermidis* cells exposed to noncoated, Ag-SNP@TRP-coated, and Ag-CNT@TRP-coated substrates.

control, and compared with TAC-applied films (Figure 5c). The RLU values for the TACs were significantly lower that that for noncoated control, and the values further decreased when the TSP was turned on because of the enhanced effective surface area of AgNP to be diffused as Ag^+ to *E. coli*. This panel temperature-dependent activity may be explained by PNIPAM shrinkage causing release of absorbed moisture from PNIPAM matrix, and this could be associated with absorption of atmospheric humidity by PNIPAM-based nano/microgels intoduced in previous reports.[39,40] This finding implies that the TACs have potential for realistic applications even under heat-sensitive configuration (refer to the right-bottom image in Figure 1). The released Ag^+ may be diffused to react with thiol groups of the cell membrane proteins to form −S−Ag and subsequently induce pitlike conformational changes, resulting in protein leakage through the membrane.[41] To confirm this hypothesis, *S. epidermidis* and *E. coli* placed on TACs for 2 min at different temperatures were detached and transferred to 2′,7′-dichlorodihydrofluorescein diacetate assay to measure intracellular reactive oxygen species (ROS); Ag^+ can generally promote ROS production in bacteria by blocking the activity of thiol-containing antioxidative enzymes.[41,42] As shown in Figure S7, ROS generation reflected well on parameters regarding supporting materials and bacteria. In particular, damage of the cell membrane, protein, and intracellular system became severe upon the increase in temperature.

Antimicrobial activities of the TACs were further confirmed by measuring the morphological changes when *E. coli* cells were incubated on Ag-SNP@TRP- and Ag-CNT@TRP-coated TSP protection films. Field-emission SEM (S-4800, Hitach, Japan) images show morphological changes of *E. coli* when they were incubated with Ag-SNP@TRP and Ag-CNT@TRP for 1 h. Untreated *E. coli* cells kept within rodlike shapes (Figure 6a), whereas the treatments with the TANs revealed significant changes in morphology (Figure 6b,c). This implies that close contact between the cells and TANs introduced irreversible damage and disruption that led to cell death. Viable bacterial cells (green) exposed to the TACs were also analyzed using a confocal laser scanning microscope (CLSM, Leica Microsystems, Germany), as shown in Figure 6d,e. The TACs led to >83% ($p < 0.05$) decrease in the survival rate of the bacteria (*E. coli* and *S. epidermidis*) after 1 h of incubation in comparison with noncoated substrate. The results are consistent with the ATP assays, indicating that applying TACs may be a viable option to reduce bacterial contamination with frequently contacted surfaces.

To assess the biocompatibility of TANs, including TRP alone, the cytotoxicities were tested in human embryonic kidney (HEK) 293 cells using 3-(4,5-dimethylthiazol-2-yl)-5-(3-carboxymethoxyphenyl)-2-(4-sulfophenyl)-2*H*-tetrazolium (MTS) assay at a different mass concentration (10−150 $\mu g\ mL^{-1}$). The results (Figure S8) show that the TANs did not introduce any significant cytotoxic effects (>80% in cell viability) at all the MIC values compared with TRP alone, which indicated that TRP on Ag-SNP or Ag-CNT efficiently prevented the burst release of Ag^+ to kill the cells because noncoated AgNPs can significantly increase cytotoxicity for mammalian cells.[43] The slightly higher cytotoxicities of Ag-CNT@TRP samples might be caused by the higher aspect ratio of CNT in shapes that perforate and/or lyse cells via needle-like action.[37] The cell viability results demonstrated that TRP incorporation not only led to heat-sensitive antimicrobial activities but also significantly reduced unwanted toxic effects of AgNPs to possess enhanced biocompatibility.

3. CONCLUSIONS

We designed and prepared a single-pass gas-to-liquid reaction system to assemble TANs and TACs in an on-demand continuous production configuration. This method involved continuous production of aerosol SNPs and CNTs via spark ablation and their successive injection into liquid solution containing Ag^+, PNIPAM, and PDMS in the presence of ultrasound. Thermoresponsive antimicrobial activities of the TANs were first examined in bacterial culture medium at different temperatures (27 and 37 °C), and the TACs were employed on TSP protective films with turned-on (38.1 °C) and -off (23.8 °C) modes to determine their potential for realistic applications. TRP incorporation not only offered heat-sensitive antimicrobial activity but also reduced unwanted toxic effects of AgNPs for their efficient applications. This newly

DOI: 10.1021/acsami.7b05167
ACS Appl. Mater. Interfaces 2017, 9, 15342−15349

developed approach provides novel perspectives and useful information for realizable fabrication route and platform to a broad range of antimicrobial applications.

■ ASSOCIATED CONTENT

Supporting Information

The Supporting Information is available free of charge on the ACS Publications website at DOI: 10.1021/acsami.7b05167.

Experimental details, XRD profiles of SNPs and CNTs, XPS spectra of nanocomposites, UV−vis and FTIR spectra of nanocomposites including SNPs and CNTs, size distributions of SNPs, CNTs, and TRP particles (25 and 37 °C), adsorption isotherms of the nanocomposites, ROS generation and cell cytotoxicity measurement of nanocomposites, and summaries of size distributions of nanocomposites including TRP, SNPs, and CNTs (with and without ultrasound) (PDF)

■ AUTHOR INFORMATION

Corresponding Authors

*E-mail: postjb@yu.ac.kr (J.H.B.).
*E-mail: park895@purdue.edu (J.H.P).

ORCID

Jeong Hoon Byeon: 0000-0003-0903-7128

Notes

The authors declare no competing financial interest.

■ ACKNOWLEDGMENTS

This work was supported by the National Research Foundation of Korea Grant funded by the Korean Government (NRF-2015R1A2A2A04005809).

■ REFERENCES

(1) Brady, R. R.; Verran, J.; Damani, N. N.; Gibb, A. P. Review of Mobile Communication Devices as Potential Reservoirs of Nosocomial Pathogens. *J. Hosp. Infect.* **2009**, *71*, 295−300.

(2) Kiedrowski, L. M.; Perisetti, A.; Loock, M. H.; Khaitsa, M. L.; Guerrero, D. M. Disinfection of iPad to Reduce Contamination with Clostridium Difficile and Methicillin-Resistant Staphylococcus Aureus. *Am. J. Infect. Control* **2013**, *41*, 1136−1137.

(3) Singh, S.; Acharya, S.; Bhat, M.; Rao, S. K.; Pentapati, K. C. Mobile Phone Hygiene: Potential Risks Posed by Use in the Clinics of an Indian Dental School. *J. Dent. Educ.* **2010**, *74*, 1153−1158.

(4) Page, K.; Wilson, M.; Parkin, I. P. Antimicrobial Surfaces and Their Potential in Reducing the Role of the Inanimate Environment in the Incidence of Hospital-Acquired Infections. *J. Mater. Chem.* **2009**, *19*, 3819−3831.

(5) Muñoz-Bonilla, A.; Fernández-García, M. Polymeric Materials with Antimicrobial Activity. *Prog. Polym. Sci.* **2012**, *37*, 281−339.

(6) Timofeeva, L.; Kleshcheva, N. Antimicrobial Polymers: Mechanism of Action, Factors of Activity, and Applications. *Appl. Microbiol. Biotechnol.* **2011**, *89*, 475−492.

(7) Shi, Z. Q.; Cai, Y. T.; Deng, J.; Zhao, W. F.; Zhao, C. S. Host-Guest Self-Assembly Toward Reversible Thermoresponsive Switching for Bacteria Killing and Detachment. *ACS Appl. Mater. Interfaces* **2016**, *8*, 23523−23532.

(8) Siedenbiedel, F.; Tiller, J. C. Antimicrobial Polymers in Solution and on Surfaces: Overview and Functional Principles. *Polymers* **2012**, *4*, 46−71.

(9) Muñoz-Bonilla, A.; Fernández-García, M. The Roadmap of Antimicrobial Polymeric Materials in Macromolecular Nanotechnology. *Eur. Polym. J.* **2015**, *65*, 46−62.

(10) Cloutier, M.; Mantovani, D.; Rosei, F. Antibacterial Coatings: Challenges, Perspectives, and Opportunities. *Trends Biotechnol.* **2015**, *33*, 637−652.

(11) Kim, J. S.; Kuk, E.; Yu, K. N.; Kim, J.-H.; Park, S. J.; Lee, H. J.; Kim, S. H.; Park, Y. K.; Park, Y. H.; Hwang, C.-Y.; Kim, Y.-K.; Lee, Y.-S.; Jeong, D. H.; Cho, M.-H. Antimicrobial Effects of Silver Nanoparticles. *Nanomedicine* **2007**, *3*, 95−101.

(12) Knetsch, M. L. W.; Koole, L. H. New Strategies in the Development of Antimicrobial Coatings: The Example of Increasing Usage of Silver and Silver nanoparticles. *Polymers* **2011**, *3*, 340−366.

(13) Chopra, I. The Increasing Use of Silver-Based Products as Antimicrobial Agents: A Useful Development or a Cause for Concern? *J. Antimicrob. Chemother.* **2007**, *59*, 587−590.

(14) Furno, F.; Morley, K. S.; Wong, B.; Sharp, B. L.; Arnold, P. L.; Howdle, S. M.; Bayston, R.; Brown, P. D.; Winship, P. D.; Reid, H. J. Silver Nanoparticles and Polymeric Medical Devices: A New Approach to Prevention of Infection? *J. Antimicrob. Chemother.* **2004**, *54*, 1019−1024.

(15) Mijnendonckx, K.; Leys, N.; Mahillon, J.; Silver, S.; Van Houdt, R. Antimicrobial Silver: Uses, Toxicity and Potential for Resistance. *BioMetals* **2013**, *26*, 609−621.

(16) Caballero-Díaz, E.; Pfeiffer, C.; Kastl, L.; Rivera-Gil, P.; Simonet, B.; Valcárcel, M.; Jiménez-Lamana, J.; Laborda, F.; Parak, W. J. The Toxicity of Silver Nanoparticles Depends on Their Uptake by Cells and Thus on Their Surface Chemistry. *Part. Part. Syst. Char.* **2013**, *30*, 1079−1085.

(17) Castle, A. B.; Gracia-Espino, E.; Nieto-Delgado, C.; Terrones, H.; Terrones, M.; Hussain, S. Hydroxyl-Functionalized and N-Doped Multiwalled Carbon Nanotubes Decorated with Silver Nanoparticles Preserve Cellular Function. *ACS Nano* **2011**, *5*, 2458−2466.

(18) Pinto, V. V.; Ferreira, M. J.; Silva, R.; Santos, H. A.; Silva, F.; Pereira, C. M. Long Time Effect on the Stability of Silver Nanoparticles in Aqueous Medium: Effect of the Synthesis and Storage Conditions. *Colloids Surf., A* **2010**, *364*, 19−25.

(19) MacCuspie, R. I. Colloidal Stability of Silver Nanoparticles in Biologically Relevant Conditions. *J. Nanopart. Res.* **2011**, *13*, 2893−2908.

(20) Kvítek, L.; Panáček, A.; Soukupová, J.; Kolář, M.; Večeřová, R.; Prucek, R.; Holecová, M.; Zbořil, R. Effect of Surfactants and Polymers on Stability and Antibacterial Activity of Silver Nanoparticles (NPs). *J. Phys. Chem. C* **2008**, *112*, 5825−5834.

(21) Shao, W.; Liu, X.; Min, H.; Dong, G.; Feng, Q.; Zuo, S. Preparation, Characterization, and Antibacterial Activity of Silver Nanoparticle-Decorated Graphene Oxide Nanocomposite. *ACS Appl. Mater. Interfaces* **2015**, *7*, 6966−6973.

(22) Pramanik, S.; Hazarika, J.; Kumar, A.; Aidew, L.; Buragohain, A. K.; Karak, N. Green-Silver Nanoparticle-Decorated Multiwalled Carbon Nanotube: A Precursor for Fabrication of Multifunctional Biobased Sustainable Nanocomposites. *ACS Sustainable Chem. Eng.* **2014**, *2*, 2510−2518.

(23) Song, J.; Kim, H.; Jang, Y.; Jang, J. Enhanced Antibacterial Activity of Silver/Polyrhodanine-Composite-Decorated Silica Nanoparticles. *ACS Appl. Mater. Interfaces* **2013**, *5*, 11563−11568.

(24) Seo, Y.; Hwang, J.; Kim, J.; Jeong, Y.; Hwang, M. P.; Choi, J. Antibacterial Activity and Cytotoxicity of Multi-Walled Carbon Nanotubes Decorated with Silver Nanoparticles. *Int. J. Nanomed.* **2014**, *9*, 4621−4629.

(25) Vihola, H.; Laukkanen, A.; Tenhu, H.; Hirvonen, J. Drug Release Characteristics of Physically Cross-Linked Thermosensitive Poly(*N*-vinylcaprolactam) Hydrogel Particles. *J. Pharm. Sci.* **2008**, *97*, 4783−4793.

(26) Twaites, B. R.; de Las Heras Alarcón, C.; Lavigne, M.; Saulnier, A.; Pennadam, S. S.; Cunliffe, D.; Górecki, D. C.; Alexander, C. Thermoresponsive Polymers as Gene Delivery Vectors: Cell Viability, DNA Transport and Transfection Studies. *J. Controlled Release* **2005**, *108*, 472−483.

(27) Doorty, K. B.; Golubeva, T. A.; Gorelov, A. V.; Rochev, Y. A.; Allen, L. T.; Dawson, K. A.; Gallagher, W. M.; Keenan, A. K. Poly(*N*-isopropylacrylamide) Co-Polymer Films as Potential Vehicles for

DOI: 10.1021/acsami.7b05167
ACS Appl. Mater. Interfaces 2017, 9, 15342−15349

Delivery of an Antimitotic Agent to Vascular Smooth Muscle Cells. *Cardiovasc. Pathol.* **2003**, *12*, 105−110.
(28) James, C.; Johnson, A. L.; Jenkins, A. T. Antimicrobial Surface Grafted Thermally Responsive PNIPAM-*co*-ALA Nano-Gels. *Chem. Commun.* **2011**, *47*, 12777−12779.
(29) Laloyaux, X.; Fautré, E.; Blin, T.; Purohit, V.; Leprince, J.; Jouenne, T.; Jonas, A. M.; Glinel, K. Temperature-Responsive Polymer Brushes Switching from Bactericidal to Cell-Repellent. *Adv. Mater.* **2010**, *22*, 5024−5028.
(30) Ward, M. A.; Georgiou, T. K. Thermoresponsive Polymers for Biomedical Applications. *Polymers* **2011**, *3*, 1215−1242.
(31) Zafar, M.; Shah, T.; Rawal, A.; Siores, E. Preparation and Characterisation of Thermoresponsive Nanogels for Smart Antibacterial Fabrics. *Mater. Sci. Eng., C* **2014**, *40*, 135−141.
(32) Byeon, J. H.; Kim, J.-W. Production of Carbonaceous Nanostructures from a Silver-Carbon Ambient Spark. *Appl. Phys. Lett.* **2010**, *96*, 153102.
(33) Sun, X.; Dong, S.; Wang, E. One-Step Preparation and Characterization of Poly(propyleneimine) Dendrimer-Protected Silver Nanoclusters. *Macromolecules* **2004**, *37*, 7105−7108.
(34) Kusolkamabot, K.; Sae-ung, P.; Niamnont, N.; Wongravee, K.; Sukwattanasinitt, M.; Hoven, V. P. Poly(*N*-isopropylacrylamide)-Stabilized Gold Nanoparticles in Combination with Tricationic Branched Phenylene-Ethynylene Fluorophore for Protein Identification. *Langmuir* **2013**, *29*, 12317−12327.
(35) Cruz-Delgado, V. J.; España-Sánchez, B. L.; Avila-Orta, C. A.; Medellín-Rodríguez, F. J. Nanocomposites Based on Plasma-Polymerized Carbon Nanotubes and Nylon-6. *Polym. J.* **2012**, *44*, 952−958.
(36) Byeon, J. H.; Hwang, J. Morphology of Metallic Nanoparticles as a Function of Deposition Time in Electroless Deposition of Metal on Multi-Walled Carbon Nanotubes. *Surf. Coat. Technol.* **2008**, *203*, 357−363.
(37) Chen, H.; Wang, B.; Gao, D.; Guan, M.; Zheng, L.; Ouyang, H.; Chai, Z.; Zhao, Y.; Feng, W. Broad-Spectrum Antibacterial Activity of Carbon Nanotubes to Human Gut Bacteria. *Small* **2013**, *9*, 2735−2746.
(38) Kim, S.-H.; Lee, H.-S.; Ryu, D.-S.; Choi, S.-J.; Lee, D.-S. Antibacterial Activity of Silver-Nanoparticles Against *Staphylococcus Aureus* and *Escherichia Coli*. *Kor. J. Microbiol. Biotechnol.* **2011**, *39*, 77−85.
(39) Islam, M. R.; Li, X.; Smyth, K.; Serpe, M. J. Polymer-Based Muscle Expansion and Contraction. *Angew. Chem., Int. Ed.* **2013**, *52*, 10330−10333.
(40) Islam, M. R.; Serpe, M. J. Poly(N-Isopropylacrylamide) Microgel-Based Thin Film Actuators for Humidity Sensing. *RSC Adv.* **2014**, *4*, 31937−31940.
(41) Gordon, O.; Slenters, T. V.; Brunetto, P. S.; Villaruz, A. E.; Sturdevant, D. E.; Otto, M.; Landmann, R.; Fromm, K. M. Silver Coordination Polymers for Prevention of Implant Infection: Thiol Interaction, Impact on Respiratory Chain Enzymes, and Hydroxyl Radical Induction. *Antimicrob. Agents Chemother.* **2010**, *54*, 4208−4218.
(42) Park, H.-J.; Kim, J. Y.; Kim, J.; Lee, J.-H.; Hahn, J.-S.; Gu, M. B.; Yoon, J. Silver-Ion-Mediated Reactive Oxygen Species Generation Affecting Bactericidal Activity. *Water Res.* **2009**, *43*, 1027−1032.
(43) Byeon, J. H. Scalable Hybrid Chemical Manufacture to Photothermal Therapy: PEG-Capped Phototransducers. *Sci. Rep.* **2016**, *6*, 31351.

DOI: 10.1021/acsami.7b05167
ACS Appl. Mater. Interfaces 2017, 9, 15342−15349